

## Importance of Schottky barriers for wide-bandgap thermoelectric devices

M. Wais,<sup>1,\*</sup> K. Held,<sup>1</sup> and M. Battiato<sup>2</sup>

<sup>1</sup>*Institute for Solid State Physics, TU Wien, Vienna, Austria*

<sup>2</sup>*Nanyang Technological University, 21 Nanyang Link, Singapore, Singapore*



(Received 20 October 2017; published 17 April 2018)

The development of thermoelectric devices faces not only the challenge of optimizing the Seebeck coefficient, the electrical and thermal conductivity of the active material, but also further bottlenecks when going from the thermoelectric material to an actual device, e.g., the dopant diffusion at the hot contact. We show that for large bandgap thermoelectrics another aspect can dramatically reduce the efficiency of the device: the formation of Schottky barriers. Understanding the effect, it can then be fixed rather cheaply by a two-metal contact solution.

DOI: [10.1103/PhysRevMaterials.2.045402](https://doi.org/10.1103/PhysRevMaterials.2.045402)

### I. INTRODUCTION

In recent years, vast scientific efforts have been invested in increasing the performance of thermoelectric devices [1]. Already a number of very attractive applications for sustainable energy solutions [2] and technological applications such as Peltier coolers, heat pumps [3], microscopic generators [4], and probes for quality control of solid state devices [5] are being pursued. But for widespread applications more efficient thermoelectric devices are badly needed.

The development and optimization of a thermoelectric device is a task that requires tuning a number of parameters. The choice of a material which excels in interrelated and often competing thermoelectric properties is imperative. That is, one is searching for materials with a large Seebeck coefficient which has, at the same time, a good electric and low thermal conductance. This has triggered an intensive quest for new higher performing materials [2,6–10].

However, even highly promising materials can struggle to find application in commercial devices due to deficiencies in auxiliary properties that become important when going from the bulk thermoelectric material to an actual device. Several such properties have been identified and discussed in the literature: proneness to interdiffusion [11–13], lack of chemical stability and resistance to oxidation [14], poor mechanical properties or low resistance to mechanical stresses [15], a too broad temperature dependence of the thermal expansion coefficient [16], a low resistance to heat or a low melting point, as well as toxicity. New thermoelectric materials such as oxide thermoelectrics [17–21] may excel over traditional semiconductors in many of the mentioned properties.

In this work we show that for wide-bandgap materials, an arguably even more important effect is the formation of Schottky barriers which can dramatically reduce the efficiency of the thermoelectric device. While the importance of Schottky barriers for semiconducting electronics is well established [22], its role for thermoelectric devices has been by and large overlooked in the literature. Neither is it taken into account in simulations for the thermoelectric efficiency [23,24], except

sometimes indirectly as a (constant) contact resistance of unknown origin [25–29]. Noteworthy and consistent with our findings, the experimental contact resistance appears to be particularly critical for wide-bandgap thermoelectric materials [17,30,31], making their performance consistently worse than expected [27]. This is a very problematic issue, since it discourages the pursuit of otherwise very promising materials.

In our paper, we compute these losses. Understanding that the formation of a Schottky barrier plays an essential role, we propose a simple and inexpensive way to mend the effect using a two-metal contact. Experimentally such a setup might have been achieved in some cases by chance, when engineering the contacts of the thermoelectric device by trial and error.

Our calculations use the standard charge and heat transport equations [32], but beyond the dependence on the temperature considered before we explicitly include also the dependence of all the transport properties on the chemical potential. The latter is essential to describe the Schottky barrier and has been considered for semiconductor electronics, but there in turn the temperature dependence is not relevant and has been discarded.

In the following, we first introduce the relevant equations. We then apply the treatment to two different materials for illustrative purposes. We compare for the small-bandgap thermoelectric material  $\text{Bi}_2\text{Te}_3$ , our treatment with the most commonly used estimations of the efficiency, showing how both standard estimations and more advanced ones [24,28] overestimate the device efficiency. Finally we apply our method to the large-bandgap thermoelectric  $\text{SrTiO}_3$ . We conclude that if the two branches of the thermoelectric device are formed by the same but differently doped active material, a single-metal contact is insufficient to avoid the formation of a Schottky barrier. We show that and how the contacts have to be composed by two different metals to prevent it. The reader should notice, however, that several other sources of loss can critically compromise junctions or the performance of thermoelectric devices.

### II. THEORY AND METHOD

For the theoretical description, we assume an effective one-dimensional device consisting of two active regions (green and

\*michael.wais@tuwien.ac.at

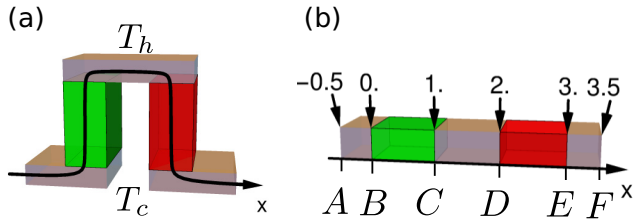


FIG. 1. (a) Schematic picture of a thermoelement. The red and green areas are thermoelectric materials and the grey areas are metals held at temperatures  $T_h$  and  $T_c$ . (b) Corners are neglected and the device is treated as an effective one-dimensional device. The junctions are labeled from A to F; positions are given in mm.

red areas in Fig. 1) which are connected by metallic contacts held at different temperatures  $T_h$  (hot side) and  $T_c$  (cold side). The coordinate  $x$  represents the position across the device. As already pointed out we maintain the full dependence of the transport coefficients on the temperature  $T$  and the chemical potential  $\mu$ . The Seebeck coefficient  $S$ , the charge density  $\rho$ , the electrical  $\sigma$ , and thermal conductivity  $\kappa$  depend on the material considered as well as on  $T$  and  $\mu$  (and doping):

$$S(x) = S(\mu(x), T(x)), \quad \rho(x) = \rho(\mu(x), T(x)), \quad (1)$$

$$\sigma(x) = \sigma(\mu(x), T(x)), \quad \kappa(x) = \kappa(\mu(x), T(x)), \quad (2)$$

where we have highlighted that these are position dependent through the (yet to be determined) position dependence of  $T(x)$  and  $\mu(x)$ .

Within the active regions, three equations are necessary to determine  $T(x)$ ,  $\mu(x)$ , as well as the electrical potential profile  $\phi(x)$  [1]:

$$j = -\sigma(x) \left( \phi'(x) - \frac{1}{e} \mu'(x) + S(x) T'(x) \right), \quad (3)$$

$$\frac{j^2}{\sigma(x)} + \kappa'(x) T'(x) + \kappa(x) T''(x) - T(x) j S'(x) = 0, \quad (4)$$

$$\phi''(x) = -\frac{\rho(x)}{\epsilon_0 \epsilon}. \quad (5)$$

Here,  $j$  is the charge current,  $\epsilon_0 \epsilon$  the dielectric constant of the material, and  $e$  the absolute value of the electron charge. The first equation is the macroscopic charge transport equation where charge conservation is imposed by enforcing a spatially constant current. The second one is the so-called Domenicali equation [33] which corresponds to energy conservation; and Eq. (5) is the Poisson equation.

Before addressing the problem numerically, we can further eliminate  $\phi(x)$  in Eq. (3) by means of Eq. (5) leading to the second-order differential equation

$$-\frac{1}{e} \mu''(x) = \frac{\rho(x)}{\epsilon_0 \epsilon} + \frac{j}{\sigma(x)^2} \sigma'(x) - [S(x) T'(x)]'. \quad (6)$$

The differential equations (4) and (6) need to be solved self-consistently together with the material-dependent properties in Eqs. (1) and (2). This yields  $\mu(x)$  and  $T(x)$  if we assign the

boundary conditions

$$T(B) = T(E) = T_c, \quad T(C) = T(D) = T_h, \quad (7)$$

$$\mu(B) = \mu(C) = \mu(D) = \mu(F) = \mu_F. \quad (8)$$

Here,  $\mu_F$  is the Fermi level of the metal contacts [34]. The one above is a very good approximation in the usual case where the density of states of the metal is much bigger than that of the active material.

Once the equations have been solved, the efficiency of the thermoelectric device can be computed as

$$\eta = \frac{P_{el}}{J_Q} = \frac{[\bar{\phi}(F) - \bar{\phi}(A)]j}{j_Q(D) - j_Q(C)}, \quad (9)$$

where  $\bar{\phi}(x) \equiv \phi(x) - \frac{1}{e} \mu(x)$  is the electrochemical potential which is equivalent to the local voltage, and

$$j_Q(x) = S(x) T(x) j - \kappa(x) T'(x) \quad (10)$$

is the heat current. To identify the maximum efficiency  $\eta_{max}$  we solve the equations for different operating conditions, characterized by different currents  $j$ .

For the examples below, the chemical-potential- and temperature-dependent transport properties of Eqs. (1) and (2) have been obtained using BOLTZTRAP [35] with band structures calculated from density functional theory (DFT) using WIEN2K [36]. The doping is treated by assuming a rigid band structure and adding the dopant ionic charge to the charge expression in Eq. (1). To obtain the transport properties from BOLTZTRAP we need the relaxation time  $\tau(T)$ , which is determined by fitting the electrical conductivity to experimental values for a given carrier concentration. Furthermore the unit cell volume is needed to get the correct charge density. For the phononic part of the thermal conductivity we assume  $\kappa_{ph}(T) = \alpha/T$  where the parameter  $\alpha$  is again determined by fitting to experiments.

We solve Eqs. (4) and (6) numerically within the two active regions using finite elements with a nonuniform mesh, determining the position dependence of the transport properties self-consistently.

Below we compare our numerical results to the most common expressions employed in the literature to estimate the maximum efficiency of a thermoelectric element. For a device with constant transport coefficients the maximum efficiency can be calculated analytically and reads

$$\eta(Z) = \eta_c \frac{\sqrt{1 + ZT_m} - 1}{\sqrt{1 + ZT_m} + T_c/T_h}, \quad (11)$$

where  $ZT_m$  is the celebrated figure of merit with  $Z = \sigma S^2/\kappa$ ;  $T_c$  ( $T_h$ ) the temperature at the cold (hot) side;  $T_m$  the mean temperature, i.e.,  $T_m = (T_h + T_c)/2$ , and  $\eta_c = (T_h - T_c)/T_h$  the Carnot efficiency.

For real devices we will compare our numerical simulations with three common approximations: (i) the efficiency given by Eq. (11) with  $Z$  evaluated at the mean temperature  $T_m$ , (ii) the efficiency given by Eq. (11) but with the temperature-averaged figure of merit  $\eta_{ii} \equiv \eta(Z = \frac{1}{T_h - T_c} \int_{T_c}^{T_h} dT \frac{S(T)^2 \sigma(T)}{\kappa(T)})$ , and (iii) the efficiency corresponding to the recently proposed engineering figure of merit  $\eta_{eng}$  [24]. Note that our treatment is more general than (iii) and yields the latter if the temperature

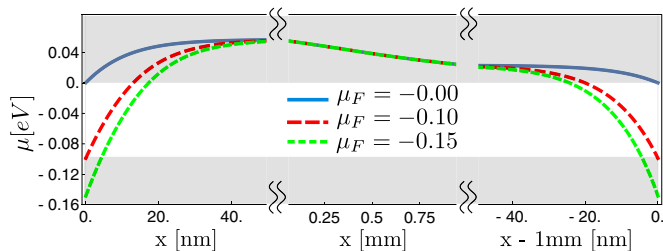


FIG. 2. Chemical potential across the  $n$ -doped  $\text{Bi}_2\text{Te}_3$  region for different chemical potential  $\mu_F$  of the contact,  $T_c = 300$  K and  $T_h = 600$  K. The current that gives the maximum efficiency (Table I) is  $j = 3.2$  A/mm<sup>2</sup> for all cases. Note the zoom in (the different length scale) at the two interfaces. The bottom of the conduction band is taken as zero point. The gray areas mark the conduction and valence band.

profile is linear [i.e.,  $T(x) = T_c + (T_h - T_c)x$  between B and C in Fig. 1 and analogously between D and E] and if one assumes that  $\mu(x)$  is everywhere at its equilibrium value.

### III. RESULTS AND DISCUSSION

#### A. $\text{Bi}_2\text{Te}_3$

We first study the case of the widely used, narrow bandgap thermoelectric material,  $n$ - and  $p$ -doped bismuth telluride ( $\text{Bi}_2\text{Te}_3$ ;  $n_{\text{dop}} = \pm 2.5 \times 10^{18}$  cm<sup>-3</sup>;  $\tau(T) = (25.05 \exp[-T/93.65] + 1.11) \times 10^{-14}$  s [37,38]; rhombohedral unit cell with  $a = 1.047$  nm and  $c = 3.048$  nm [37];  $\kappa_{\text{ph}} = 540/T$  [37];  $\epsilon = 100$  [39]), operating between the temperatures  $T_c = 300$  K,  $T_h = 600$  K. We want to compare the effect of contacting the active regions with different metals, which we model by different contact potentials  $\mu_F$ .

In Fig. 2 we plot the position dependence of the chemical potential within the  $n$ -doped arm of the device for the three cases. We find that the chemical potential within the bulk hardly deviates from its equilibrium value. However, at the junctions, it is forced to the boundary value  $\mu_F$  (left and right section of Fig. 2). In spite of the explicit chemical potential dependence of the transport properties, the change in the transport coefficients at the boundaries is not important enough to appreciably affect the efficiency. This is because the bandgap ( $E_{\text{gap}} \approx 0.11$  eV[40]) is not much larger than  $T_c$  (0.026 eV) so that there remain temperature-induced charge carriers even if the chemical potential lies within the gap, and the deviation of the chemical potential is anyhow restricted to a small region of  $O(10)$  nm.

In Table I we compare the different estimations of the efficiency for the  $n$ -doped leg with the one obtained in this work. The estimations  $\eta_i$  and  $\eta_{ii}$  are known to overestimate

TABLE I. Comparison of the different efficiency estimations and the simulations.

	$\eta_i$	$\eta_{ii}$	$\eta_{\text{eng}}$ [24]	$\eta_{\text{sim}}$		
$\text{Bi}_2\text{Te}_3$				$\mu_F = 0$	$\mu_F = -0.1$	$\mu_F = -0.15$
	5.34%	5.11%	4.94%	4.85%	4.85%	4.85%
$\text{SrTiO}_3$				$\mu_F = 0$	$\mu_F = -0.5$	$\mu_F = -1$
	1.64%	1.58%	1.52%	1.57%	1.1%	$1.61 \times 10^{-5}\%$

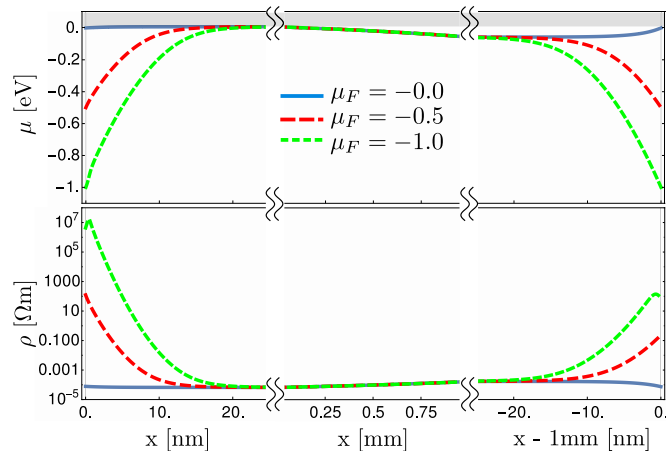


FIG. 3. Chemical potential as in Fig. 2 and the corresponding specific resistivity of  $n$ -doped  $\text{SrTiO}_3$ . The applied temperatures are  $T_c = 400$  K and  $T_h = 700$  K. The currents that give the maximum efficiency (Table I) are  $j = 400$  mA/mm<sup>2</sup> (blue),  $j = 280$  mA/mm<sup>2</sup> (red), and  $j = 5.6$   $\mu\text{A/mm}^2$  (green). Note that the bandgap of the simulation is smaller than in reality ( $E_{\text{gap}} \approx 1.9$  eV).

the efficiency, which is confirmed here. The efficiency estimation from Ref. [24] agrees better with the simulated values. The remaining deviation is due to the nonlinear temperature distribution in the real system.

#### B. $\text{SrTiO}_3$

The situation is entirely different in doped strontium titanate ( $\text{SrTiO}_3$ ;  $n_{\text{dop}} = \pm 10^{20}$  cm<sup>-3</sup>;  $\tau(T) = (10.125 \exp[-T/493.261] - 1) \times 10^{-14}$  s obtained by fitting to data in Ref. [41];  $\kappa_{\text{ph}} = 1600/T$  obtained by fitting to data in Ref. [42]; cubic unit cell with  $a = 0.3905$  nm [42];  $\epsilon \approx 288$  at room temperature[43]), which is a high bandgap material with admirable thermoelectric properties [42]. We again compare the running conditions for three different values of  $\mu_F$ . In all three cases the temperature slope is almost linear (not shown). When the metal's Fermi level lies at the bottom of the conduction band, we find excellent agreement between  $\eta_i$ ,  $\eta_{ii}$ ,  $\eta_{\text{eng}}$  and the simulation (first four columns in Table I). This is understandable since the transport properties do not vary strongly with temperature so all the approaches become equivalent.

On the other hand the efficiency dramatically drops if the metal's Fermi level lies deep within the bandgap. The reason for this is the formation of a Schottky barrier and an associated depletion region (widened by the large dielectric constant in  $\text{SrTiO}_3$ ). This creates a highly resistive region close to the interface where  $\mu(x)$  lies within the now much larger bandgap (see Fig. 3). This depletion region makes the total electrical resistivity of the layer comparable to the resistivity of the rest of the device [44]. As Table I demonstrates, the Schottky barrier can even completely suppress the thermoelectric efficiency of a  $\text{SrTiO}_3$ -based device. Because of its much smaller bandgap, this effect is negligibly small for  $\text{Bi}_2\text{Te}_3$ .

The right panel of Fig. 4 shows the electrochemical potential throughout the whole device. From left to right,  $\bar{\phi}(x)$  is almost constant within the (highly conducting) metal contact. At the interface ( $x = 0$ ) there is very sharp drop (note that the

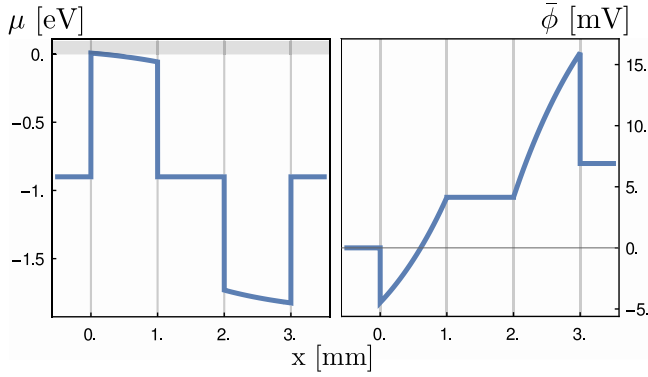


FIG. 4. Chemical potential and electrochemical potential along the whole SrTiO<sub>3</sub>-based device for metallic contacts corresponding to  $\mu_F = -0.9$  eV and  $j = 25$   $\mu\text{A}/\text{mm}^2$  which gives an efficiency of  $\eta = 6.7 \times 10^{-5}\%$ . At the cold contacts ( $x = 0$  and  $3$  mm) we observe a drop in the electrochemical potential due to the increased resistivity.

depletion region is much smaller than the dimension of the active element). Within the thermoelectric element a voltage is built. At the hot contact ( $x = 1$  mm) there is no discernible drop. This is due to the natural dependence of the conductivity of a semiconductor on the temperature. A higher temperature allows more thermally excited carriers, even when the chemical potential is within the bandgap, dramatically reducing the resistance of the Schottky barrier. A similar behavior is observed at the other branch of the device at  $x = 3$  mm. The voltage drops at the cold interfaces lead to a much smaller voltage difference across the thermoelectric device (from  $x = -0.5$  to  $3.5$  mm), and hence a loss of produced power.

Notice that due to the nonequilibrium position of the chemical potential at the junctions, the Seebeck coefficient and the thermal conductivity change as well. However, this has negligible influence on the efficiency since the change of  $\mu(x)$  is restricted to a tiny region and the Seebeck coefficient is affected almost linearly and the phononic part of the thermal conductivity is not influenced at all. The reader should notice how the usual estimations for the efficiency dramatically fail in recognizing this behavior (Table I).

### C. Two-metal contact solution

The dramatic drop in efficiency due to the formation of a Schottky barrier is therefore important in large-bandgap materials and especially at the cold side. The first obvious approach to the problem would be to select a metal with an appropriate chemical potential. However, often the two legs of a thermoelectric device consist of the same material but with opposite doping. In that case the metal used for the cold side would contact both the  $n$ - and the  $p$ -doped active regions. If the Fermi level is chosen to be optimal for one side, it will instead be extremely disadvantageous for the other side. This can be bypassed by using two different metals as shown in Fig. 5 (notice that no depletion regions are created at a metal-metal junction). Another possible solution would be to highly dope the regions around the cold junctions, leading to a faster decay of the depletion regions [22]. The reader might be led to believe that only the optimization of the cold contact is required. However, our simulations show that that is not the case. By

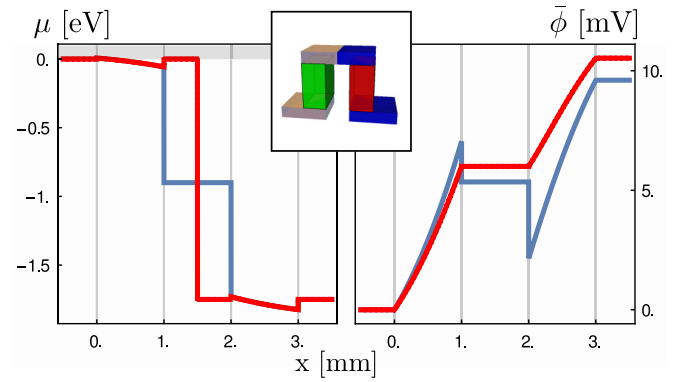


FIG. 5. Same as Fig. 4 but with different metallic contacts for each leg. Two cases are shown, one where only the cold contact has been optimized (blue) and one where both contacts are optimized (red). One can see that there is a drop in the electrochemical potential at the hot side for the blue case and no drop at all for the red one. The currents and corresponding efficiencies are  $j = 150$   $\text{mA}/\text{mm}^2$ ,  $\eta = 0.7\%$  (blue); and  $j = 250$   $\text{mA}/\text{mm}^2$ ,  $\eta = 1.22\%$  (red). The inset shows a schematic picture of the device where both contacts are optimized (red case).

the cold contact optimization the device can now run at higher currents, where usually higher efficiencies can be achieved. However, the presence of a Schottky barrier at the hot contact (even if less effective than the one at the cold side) still imposes important voltage losses and prevents reaching the maximum efficiency (Fig. 5).

## IV. CONCLUSION

In conclusion, we have performed simulations of thermoelectric generators with the full dependence of the transport coefficients on temperature and chemical potential. We found that one cannot always neglect the explicit dependence of the transport properties on the chemical potential in large bandgap materials because a disadvantageous position can lead to the formation of Schottky barriers which completely destroys the performance of the thermoelectric generator. We propose to use two different metals, separately optimized for the two ( $n$ - and  $p$ -doped) branches. The advantage of properly engineering the contacts is critical for large-bandgap thermoelectric materials, while requiring quite inexpensive adjustments of the design of the device.

Finally, we would like to remind the reader of Mahan's famous  $10k_B T$  formula, i.e., that the thermoelectric material should have a gap size of 10 times the operating temperature. However, the actual calculation [45,46] only gives a lower bound, i.e., the gap should be larger than  $10k_B T$  but no upper bound ( $ZT$  still increases insignificantly). One might speculate that at least one important reason why larger bandgap materials typically under perform, making the lower bound also the upper bound, is the formation of Schottky barriers in wide-bandgap thermoelectrics.

*Note added.* Recently we learned of a somewhat related work [47] that models a depletion region at a grain boundary by a constant shift of the chemical potential in a region of fixed width.

## ACKNOWLEDGMENTS

The authors thank V. Zlatic and E. Bauer for discussions and acknowledge financial support by the European Research Council/ERC through Grant Agreement No. 306447 and by

the Austrian Science Fund (FWF) through SFB ViCoM F41 and graduate school W1243 Solid4Fun. M. Battiato acknowledges the Austrian Science Fund (FWF) through Lise Meitner position M1925-N28 and Nanyang Technological University, NAP-SUG for funding.

- [1] V. Zlatic and R. Monnier, *Modern Theory of Thermoelectricity* (Oxford University, Oxford, 2014).
- [2] G. J. Snyder and E. S. Toberer, *Nat. Mater.* **7**, 105 (2008).
- [3] J. P. Heremans, M. S. Dresselhaus, L. E. Bell, and D. T. Morelli, *Nat. Nanotech.* **8**, 471 (2013).
- [4] S. Donsa, S. Andergassen, and K. Held, *Phys. Rev. B* **89**, 125103 (2014).
- [5] S. Cho, S. D. Kang, W. Kim, E.-S. Lee, S.-J. Woo, K.-J. Kong, I. Kim, H.-D. Kim, T. Zhang, J. A. Stroschio, Y.-H. Kim, and H.-K. Lyeo, *Nat. Mater.* **12**, 913 (2013).
- [6] M. Dresselhaus, G. Chen, M. Tang, R. Yang, H. Lee, D. Wang, Z. Ren, J.-P. Fleurial, and P. Gogna, *Adv. Mater.* **19**, 1043 (2007).
- [7] J. Yang, L. Xi, W. Qiu, L. Wu, X. Shi, L. Chen, J. Yang, W. Zhang, C. Uher, and D. J. Singh, *npj Computational Materials* **2**, 15015 (2016).
- [8] M. Battiato, J. M. Tomczak, Z. Zhong, and K. Held, *Phys. Rev. Lett.* **114**, 236603 (2015).
- [9] P. Sun, B. Wei, J. Zhang, J. M. Tomczak, A. M. Strydom, M. Søndergaard, B. B. Iversen, and F. Steglich, *Nat. Commun.* **6**, 7475 (2015).
- [10] C. Gayner and K. K. Kar, *Prog. Mater. Sci.* **83**, 330 (2016).
- [11] B. Uberuaga, G. Henkelman, H. Jónsson, S. Dunham, W. Windl, and R. Stumpf, *Phys. Status Solidi B* **233**, 24 (2002).
- [12] H. A. Bracht, H. H. Silvestri, and E. E. Haller, *Solid State Commun.* **133**, 727 (2005), Isotopic Effects in Semiconductors.
- [13] N.-H. Bae, S. Han, K. E. Lee, B. Kim, and S.-T. Kim, *Curr. Appl. Phys.* **11**, S40 (2011).
- [14] Z. Xu, Z. Lan, G. Zhu, K. Sun, and Z. Yu, *J. Alloy Comp.* **538**, 11 (2012).
- [15] V. Prokhorov and G. Pivovarov, *Ultrasonics* **51**, 715 (2011).
- [16] M.-J. Huang, P.-K. Chou, and M.-C. Lin, *Sensor Actuator Phys.* **126**, 122 (2006).
- [17] I. Matsubara, R. Funahashi, T. Takeuchi, S. Sodeoka, T. Shimizu, and K. Ueno, *Appl. Phys. Lett.* **78**, 3627 (2001).
- [18] S. Ohta, T. Nomura, H. Ohta, and K. Koumoto, *J. Appl. Phys.* **97**, 034106 (2005).
- [19] H. Ohta, *Mater. Today* **10**, 44 (2007).
- [20] X. Y. Lu, J. R. Sun, A. D. Wei, W. W. Gao, D. S. Shang, J. Wang, Z. H. Wang, and B. G. Shen, *Appl. Phys. Lett.* **97**, 022502 (2010).
- [21] Y. Lin, C. Norman, D. Srivastava, F. Azough, L. Wang, M. Robbins, K. Simpson, R. Freer, and I. A. Kinloch, *ACS Appl. Mater. Interfaces* **7**, 15898 (2015).
- [22] S. M. Sze and K. N. Kwok, *Physics of Semiconductor Devices* (Wiley-Interscience, Hoboken, NJ, 2007).
- [23] P. García-Fernández, M. Verissimo-Alves, D. I. Bilc, P. Ghosez, and J. Junquera, *Phys. Rev. B* **86**, 085305 (2012).
- [24] S. H. Kim, W. Liu, G. Chen, C.-W. Chu, and Z. Ren, *Proc. Natl. Acad. Sci. USA* **112**, 8205 (2015).
- [25] D. M. Rowe and G. Min, *IEE Proc. Sci. Meas. Technol.* **143**, 351 (1996).
- [26] S. R. Annapragada, T. Salamon, P. Kolodner, M. Hodes, and S. V. Garimella, *IEEE Trans. Compon. Packag. Manuf. Tech.* **2**, 668 (2012).
- [27] D. K. Aswal, R. Basu, and A. Singh, *Energy Convers. Manage.* **114**, 50 (2016).
- [28] H. S. Kim, W. Liu, and Z. Ren, *Energy Environ. Sci.* **10**, 69 (2017).
- [29] To the best of our knowledge the only actual calculations of thermoelectric devices including Schottky barriers beyond a mere contact resistance of arbitrary origin are in the context of high carrier infection. See the following references: [48–50]. The aim is to boost the electron-hole asymmetry to increase the thermopower (but the authors concluded that that strategy does not work). We highlight that that treatment works only in the ballistic regime, and therefore is not applicable to devices larger than  $\mu\text{m}$ . Finally that treatment disregards the temperature profile within the thermoelectric, and if applied to a whole device, it would fail to provide the physical insight that our work reaches.
- [30] Y. Cui, S. Yin, D. Wang, G. Xing, S. Leng, and R. Wang, *J. Appl. Phys.* **108**, 104506 (2010).
- [31] Y. Wang, X. Shi, X. Lai, Z. Gao, L. Liu, Y. Wang, W. Zhu, C. Meng, and L. Zhang, *Appl. Phys. Lett.* **108**, 192102 (2016).
- [32] M. Battiato, V. Zlatic, and K. Held, *Phys. Rev. B* **95**, 235137 (2017).
- [33] C. A. Domenicali, *Rev. Mod. Phys.* **26**, 237 (1954).
- [34] Note that  $\mu_F$  in reality deviate somewhat from the actual Fermi level of the metal because of, e.g., impurities at the interface or charging of the first atomic layer on the metal side.
- [35] G. K. H. Madsen and D. J. Singh, *Comput. Phys. Commun.* **175**, 67 (2006).
- [36] P. Blaha, K. Schwarz, G. Madsen, D. Kvasnicka, and J. Luitz, WIEN2K, *an augmented plane wave + local orbitals program for calculating crystal properties* (Karlheinz Schwarz, Techn. Universität Wien, Austria, 2001).
- [37] B.-L. Huang and M. Kaviani, *Phys. Rev. B* **77**, 125209 (2008).
- [38] J. Zhang, H. J. Liu, L. Cheng, J. Wei, J. Shi, X. F. Tang, and C. Uher, *J. Appl. Phys.* **116**, 023706 (2014).
- [39] L. I. Berger, *Semiconductor Materials* (CRC Press, Boca Raton, FL, 1997).
- [40] T. J. Scheidemantel, C. Ambrosch-Draxl, T. Thonhauser, J. V. Badding, and J. O. Sofo, *Phys. Rev. B* **68**, 125210 (2003).
- [41] A. Kinaci, C. Sevik, and T. Cagin, *Phys. Rev. B* **82**, 155114 (2010).
- [42] M. Hiroaki, K. Kurosaki, and S. Yamanaka, *J. Alloy Comp.* **350**, 292 (2003).
- [43] R. Viana, P. Lunkenheimer, J. Hemberger, R. Böhmer, and A. Loidl, *Phys. Rev. B* **50**, 601 (1994).
- [44] Note that Eqs. (3) and (4) describe diffusive transport. Corrections coming from ballistic transport are neglected.
- [45] G. D. Mahan, *J. Appl. Phys.* **65**, 1578 (1989).
- [46] J. O. Sofo and G. D. Mahan, *Phys. Rev. B* **49**, 4565 (1994).

- [47] J. J. Kuo, S. D. Kang, K. Imasato, H. Tamaki, S. Ohno, T. Kannoc, and G. J. Snyder, *Energy Environ. Sci.* **11**, 429 (2018).
- [48] M. Bachmann, M. Czerner, and C. Heiliger, *Phys. Rev. B* **86**, 115320 (2012).
- [49] A. Popescu, L. M. Woods, J. Martin, and G. S. Nolas, *Phys. Rev. B* **79**, 205302 (2009).
- [50] F. Lung and D. C. Marinescu, *J. Phys. Condens. Matter* **23**, 365802 (2011).